Interfacial Behavior of Slag-Fly Ash-Red Mud Based Geopolymer Mortar with OPC Concrete Substrate: Mechanical Properties and Microstructure

Qinghui Long , Yufei Zhao * , Benben Zhang * , Huichen Yang , Zhengdong Luo , Zhengyang Li , Genbao Zhang , Kun Liu

Posted Date: 30 January 2024

doi: 10.20944/preprints202401.2123.v1

Keywords: Interfacial Behavior; Slag-fly ash-red mud; geopolymer mortar; Concrete substrate; Mechanical properties

Article

Interfacial Behavior of Slag-Fly Ash-Red Mud Based Geopolymer Mortar with OPC Concrete Substrate: Mechanical Properties and Microstructure

Qinghui Long [1], Yufei Zhao [2,*], Benben Zhang [3,*], Huichen Yang [2], Zhengdong Luo [4], Zhengyang Li [4], Genbao Zhang [5] and Kun Liu [6]

[1] Yiyang Highway and Bridge Construction Co., Ltd., Yiyang 413000, China
[2] China Institute of Water Resources and Hydropower Research, Beijing 100041, China
[3] School of Transportation, Southeast University, Nanjing 211189, China
[4] College of Civil Engineering, Xiangtan University, Xiangtan 411105, China
[5] College of Civil Engineering, Hunan City University, Yiyang 413000, China
[6] Hunan Zhitong Expressway Construction and Development Co., Ltd., Changsha 410000, China
* Correspondence: zhaoyf@iwhr.com (Y.Z.); 230238946@seu.edu.cn (B.Z.)

Abstract: Geopolymer, as a new type of solid waste-based inorganic cementitious material, exhibits outstanding Behavior in terms of physical and chemical performance, macro-mechanical properties and long-lasting stability, and features potential application development tendency in the field of repair and reinforcement of existing concrete structures. This paper investigates the interfacial Behavior of geopolymer mortar with OPC concrete substrate under different slag, fly ash and red mud mixing proportions, while cement mortar was used as a control group for the research. The interfacial bonding properties of the geopolymer mortar to the OPC concrete substrate were elaborated by carrying out split tensile test, two-sided shear test and three-point bending test. The scanning electron microscopy (SEM) and X-ray diffraction (XRD) were employed to further analyse the microstructural characteristics and physical phase components of the interfacial transition zone between the geopolymer mortar and the OPC concrete substrate. The results indicated that the compressive strength of slag-fly ash-red mud-based geopolymer mortar under different mixing ratio conditions was consistently superior to that of cement mortar. Overall, the interfacial bonding properties of the geopolymer mortar to the OPC concrete substrate gradually increased with the increment of the slag content, however, an evolutionary trend of minor enhancement followed by a gradual reduction was observed with the growth of the fly ash and red mud content.

Keywords: interfacial behavior; slag-fly ash-red mud; geopolymer mortar; concrete substrate; mechanical properties

1. Introduction

Since its introduction, concrete has been one of the most common and widely used construction materials in the field of civil engineering, mainly but not limited to industrial and civil buildings, bridges and tunnels, road traffic and water conservancy projects and other engineering construction facilities. As a result of adverse conditions such as human factors or external natural environment, concrete structures will suffer from different degrees of structural damage phenomena with the growth of service time, mainly including concrete protective layer peeling [1], surface cracking [2] and reinforcement corrosion [3]. Its makes the concrete structure load bearing capacity significantly reduced, seriously threatening the normal use and service life of the overall structure, inevitably increasing the risk of use and safety hazards. The deterioration of concrete structures is mainly attributed to changing and alternating loads (fatigue loading, traffic loading, overload bearing [4–6]), attack of the external environment (carbonation, chemical ion attack, wet-dry and freeze-thaw cycles [7–9]), and structural deformation (shrinkage and creep [10,11]). Therefore, it is a technical challenge for engineers in civil engineering to improve the load-bearing performance and service life of existing concrete structures through strengthening and rehabilitation measures.

 doi:10.20944/preprints202401.2123.v1

The grouting repair method is widely used in the repair and strengthening of existing concrete structures because of the advantages of good reinforcement effect, high construction efficiency, economy and adaptability [12]. Specifically, inorganic or organic repair materials are injected into the defects of existing concrete structure, through the repair materials in the process of solidification and hardening of the physical-chemical effect on the existing concrete, so as to achieve the purpose of improving the load-bearing performance and service life of the existing concrete structure. Currently, the most widely used repair materials are cement-based cementitious materials, mainly including Portland cement mortar (PCM) [13], self-compacting concrete (SCC) [14], high performance fiber reinforced concrete (HPFRC) [15], and ultra high performance concrete (UHPC) [16]. It is undeniable that cement-based cementitious materials play an important role in the field of repair and reinforcement of existing concrete structures, mainly from their good compatibility with concrete. With the concept of green and sustainable development in human society, cement-based cementitious materials have gradually exposed various types of shortcomings. As an energy-intensive industry, cement inevitably exists with the disadvantages of high energy consumption, environmental pollution and high greenhouse gas emissions, which undoubtedly increases the pressure on the ecological environment, while not conducive to sustainable human development [17]. It is reported that the cement industry releases about 7% of the total global CO_2 emissions from all industries [18]. Thus, from the viewpoint of eco-friendly and sustainable development, there are certain limitations and restrictions in using cement-based cementitious materials to repair and strengthen existing concrete structures.

As one of the current research hotspots in the field of civil engineering materials, geopolymer has received wide attention from researchers in view of the significant advantages of low carbon and environmental protection, low energy consumption, and high resource utilization rate of industrial solid waste [19]. In addition to this, previous studies have reported that the performance behavior of geopolymer is not inferior to that of ordinary Portland cement in terms of mechanical properties, durability, and high temperature resistance [20,21]. Based on the results presented above, the call for replacing cement with geopolymer in civil engineering is gaining more and more response and support from researchers. Specifically, geopolymer refers to a three-dimensional network of inorganic gelling material assembled from aluminum-oxygen tetrahedra and silica-oxygen tetrahedra formed by the dissolution, monomer reconstruction, and monomer condensation stages of precursor materials rich in active silica-alumina mineral components under the action of alkali activator [22]. One of the potential applications of geopolymer is the repair and reinforcement of existing concrete structures because of its high early strength and superior interfacial bonding characteristics.

The silica-aluminate mineral raw material, which is one of the variables, has a significant role in influencing the various properties of geopolymer. The raw material sources of silica-aluminate minerals are mainly but not limited to industrial solid wastes (blast furnace slag, fly ash [23,24]), natural minerals (metakaolin, calcined clay [25,26]), and nonferrous metal tailings (gold mine tailings, copper mine tailings [27,28]). Currently, the precursor raw materials of geopolymer applied relatively widely in the field of repair and reinforcement of existing concrete structures are mainly slag and fly ash, which are usually in the form of individual or composite. Laskar et al. [29] compared the performance of ultra-fine slag based geopolymer mortar (GPM) and Portland cement mortar (PCM) for the repair of damaged full-size reinforced concrete beam by static four point bending test. The experiment results indicated that the reinforced concrete beam repaired by PCM indicated higher load-bearing capacity and ductility compared to PCM. Gomaa et al. [30] and Zailani et al. [31] investigated the effect of calcium content on the interfacial bonding properties of fly ash based alkali-activated concrete (AAC) and ordinary Portland cement concrete (OPCC) by indoor mechanical tests such as diagonal shear test and pull-out test. The results showed that the interfacial bond strength between ACC and OPCC gradually enhanced with the increase of calcium content in fly ash, which was mainly attributed to the increase of the number of calcium based hydration gel products. Wang et al. [32] further noted that the width of the interfacial transition zone (ITZ) of geopolymer repair mortar (GRM) and ordinary Portland cement concrete (OPCC) gradually widened with increasing

calcium content in the geopolymer precursor material, resulting in a more uniform force state and better compatibility at the repair interface. In summary, it can be speculated that geopolymer mortar prepared from slag or fly ash can be applied to the repair and reinforcement of existing concrete structures with considerable strengthening effect.

As a highly alkaline waste sludge discharged from alumina production, red mud disposed of directly in landfills without treatment not only occupies land resources and causes soil salinization but also contributes to groundwater contamination that is difficult to recover [33–35]. In addition, red mud with a large specific surface area is prone to dust generation and air pollution under open accumulation condition [36]. In response to these unfavorable factors, the comprehensive utilization of red mud is mostly in the field of construction materials, mainly being used for the preparation of concrete blocks [37], sintered bricks [38], ceramic tiles [39], and concrete admixtures [40], but the comprehensive utilization of red mud by these measures is still at a relatively low level. In order to further improve the utilization of red mud, some researchers have successfully demonstrated the feasibility and applicability of the preparation of geopolymer from red mud. The literature [41–43] reported that red mud based geopolymer possess good mechanical properties, durability and performance stability. In conclusion, the preparation of red mud into geopolymer is an effective and reasonable disposal treatment measure for bauxite residues, but few studies related to the use of red mud based geopolymer for the repair and reinforcement of existing concrete structures have been reported.

In view of this, the study attempts to confirm the feasibility of slag-fly ash-red mud based geopolymer mortar (GPM) to repair and strengthen ordinary Portland cement (OPC) concrete substrate through a series of indoor mechanical tests. Firstly, The mechanical properties of GPM prepared from different precursor raw material ratios were evaluated. Then, the mechanism of the effect of precursor raw material ratio on the interfacial bond strength between GPM and OPC concrete substrate was investigated by double-sided shear test, splitting tensile test and three-point bending test. Finally, SEM and XRD were utilized to further analyze the microstructure and hydride phase composition of the interfacial transition zone between GPM and OPC concrete substrate.

2. Materials and methods

2.1. Raw materials

In this paper, slag, fly ash and red mud were selected as composite silica-aluminate raw materials for the preparation of geopolymer. The slag is S105 grade, provided by Gongyi Longze Water Purification Material Co., Ltd, the fly ash is F class low calcium fly ash, supplied by Zhengzhou Rongchang Sheng Environmental Protection Material Co., Ltd, and the red mud is the by-product of alumina extraction from bauxite by Bayer method, offered by Zhengzhou Xinyuan New Material Co., Ltd. It should be mentioned that the red mud used in the experiment should first be placed in an electric drying oven at 80 ℃ for 12 h, then crushed and ground with a jaw crusher for 3 min, and finally sieved with a 250 μm geotechnical sieve. The cement used for the preparation of concrete substrate and cement repair mortar is P.O 42.5 grade, supplied by Xiangxiang Chengmei Cement Co., Ltd. The microscopic morphology of the raw materials used in the test is shown in **Figure 1**, in which the slag particles are mostly irregular polygons with clear contours and relatively rough surfaces, with some small particles accumulated on the surface of large particles; the surface of fly ash particles is smooth and dense, constituted by spherical vitreous microbeads of different sizes; the structure of red mud is loose, with large porosity and the distribution of fine crystal particle agglomerates; the cement is composed of haphazardly distributed lumpy particles, with more internal pore defects and rough surfaces. The chemical composition (in oxide form) of the raw materials used in the experiment was characterized by X-ray fluorescence spectroscopy (XRF), as presented in **Table 1**. The coarse aggregate used for the preparation of concrete substrate was well-graded crushed stone with a maximum particle size of 10 mm and a minimum particle size of 3 mm; the fine aggregate was river sand with a fineness modulus of 2.49, which originated from Xiangjiang river in China. The water used for the whole experiment was tap water.

 doi:10.20944/preprints202401.2123.v1

Previous studies [44,45] have consistently reported that composite alkali activator tend to be more superior to the activation of silica-aluminate raw materials than a single alkali activator, specifically to enable silica-aluminate raw materials to undergo sufficient geopolymerization reaction process such as depolymerization and polycondensation, which makes the geopolymer reflect better mechanical characteristics and durability. In view of this, for reasons of rationality, reference and economy, this study used sodium silicate solution and tablet sodium hydroxide to prepare a composite alkali activator solution with a modulus of 1.2, which is consistent with the findings of related study [46]. The sodium silicate solution exhibited an initial modulus of 3.31, a BoM of 38.5 Be, and the main chemical composition of Na_2O (8.42 wt%), SiO_2 (27.84 wt%), and H_2O (63.74 wt%). The tablet sodium hydroxide is analytically pure, with a purity greater than 98%.

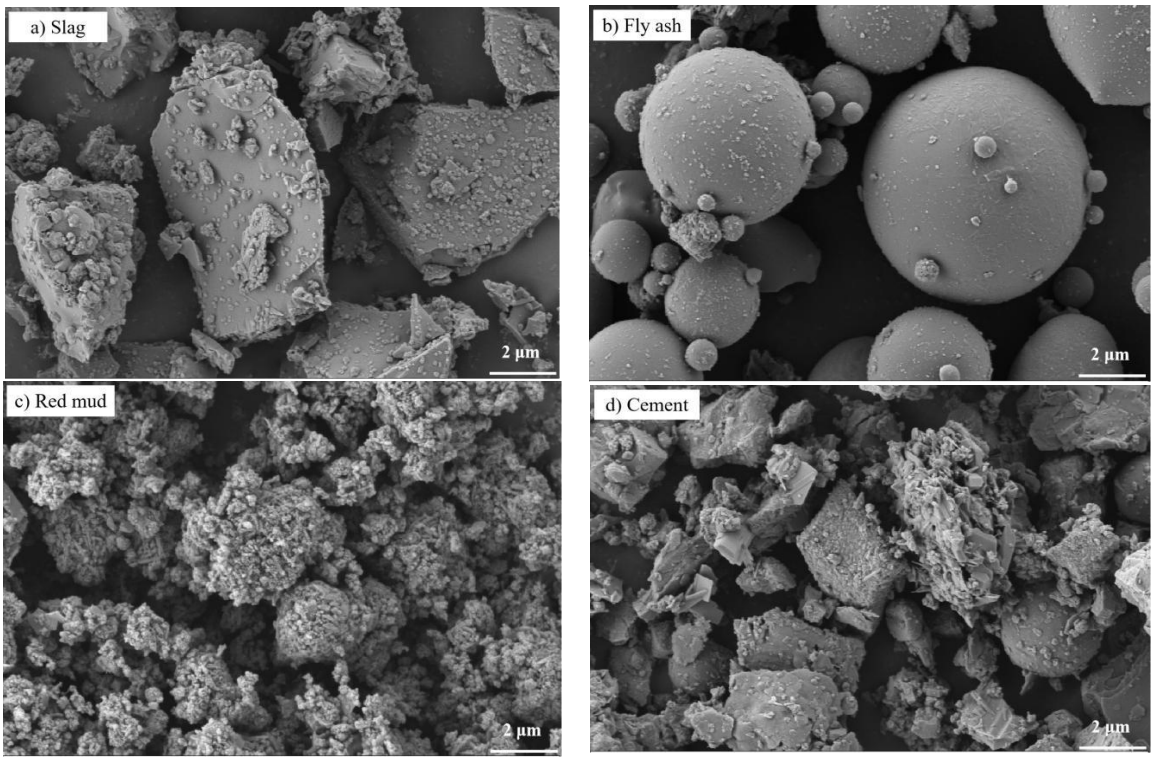

Figure 1. The SEM images of raw materials.

Table 1. The Chemical composition of raw materials (%).

	CaO	Al_2O_3	SiO_2	MgO	Fe_2O_3	SO_3	K_2O	TiO_2
Slag	35.30	16.70	34.50	5.01	1.50	1.24	-	-
Fly ash	2.32	34.70	53.04	0.86	2.53	0.35	1.76	1.25
Red mud	1.01	11.06	25.79	1.01	31.02	1.17	1.44	2.02
cement	49.20	11.52	27.50	1.18	3.38	-	-	-

2.2. OPC Concrete substrate

The OPC concrete substrate was formulated with the mass ratio of coarse aggregate: fine aggregate: cement: water as 1130: 664: 402: 205, and its design strength grade was C30. In order to investigate the interfacial bonding performance of different concrete substrate and GPM, freshly mixed concrete slurry was cast into concrete substrate of different size shapes, where the injection mold size of concrete substrates were 150 mm×150 mm×75 mm, 150 mm×150 mm×100 mm and 100 mm×100 mm×350 mm, which were tried in splitting tensile test, double-sided shear test and three-point bending test, respectively, as shown in **Figure 2**. The concrete substrates were prepared by pouring the freshly stirred concrete slurry into the corresponding concrete molds in layers, followed

 doi:10.20944/preprints202401.2123.v1

by adequate vibration and pounding, after which the concrete surface was smoothed with a scraper and placed in a room for 1 d. After completion of the curing process, the molds were demolished and the concrete substrates were transferred to a standard curing room (temperature 22±2 °C, humidity not less than 95%) for continuous curing until 28 d. In order to further exploit the mechanical interlocking effect and frictional resistance of the concrete substrate interface, and thus maximize the interfacial bonding performance between the GPM and the concrete substrate, the concrete substrate interface was roughened by mechanical grinding [47]. In view of the above expression, the roughness depth indicated by the different types of concrete substrates was regulated to 5 mm in the same way to achieve consistency in mechanical tests.

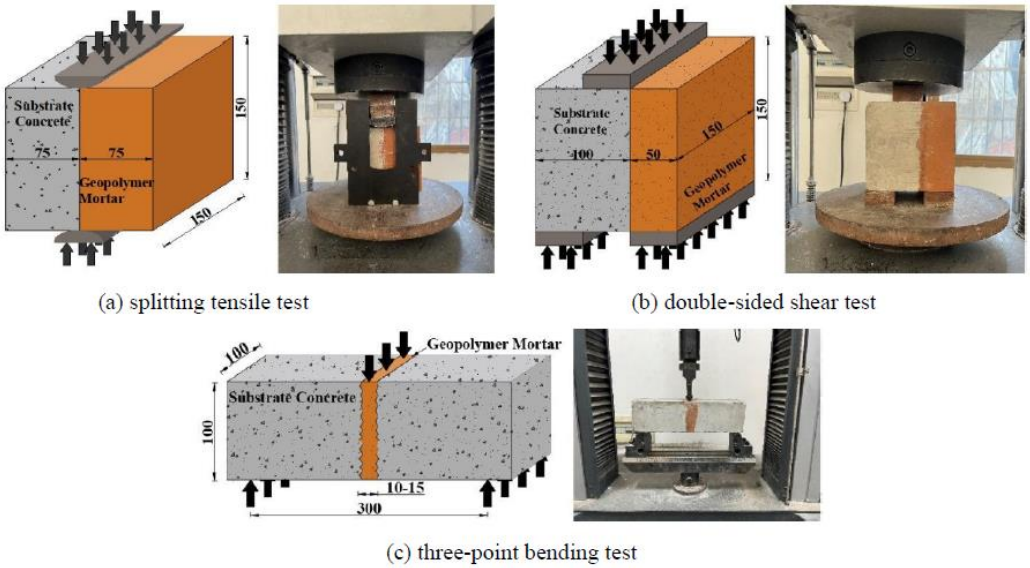

Figure 2. Interface bonding performance test between geopolymer mortar and concrete substrate.

2.3. Geopolymer mortar

The ratio scheme of the GPM is shown in **Table 2**. The design scheme of the GPM is to use slag, fly ash and red mud as unit variables respectively, and the remaining two types of silica-aluminate raw materials are blended in equal proportions, where the blending amounts of slag, fly ash and red mud are all designed to be 10%, 15%, 20% and 33%. Meanwhile, OPC mortar was adopted as the benchmark control group. The experiment process of GPM repair concrete substrate is to first put the silica-aluminate raw materials and fine aggregates together into the mixing pot and stir fully for 3 min to form a uniform mixture, then add the pre-blended alkali activator and tap water in turn and stir evenly again for 3 min to make GPM, and finally pour the GPM into the steel mold with the concrete substrate placed in advance to fully vibrate and scrape. The repaired specimens were demolded after 1 d of curing at room temperature, and then transferred to the standard curing room to continue curing until the predetermined age, after which the mechanical tests were carried out. The experiment procedure for OPC mortar repair of concrete substrate is analogous to that of geopolymer repair mortar and will not be repeated here. It is essential to emphasize that the rough surface of the concrete substrate must be thoroughly cleaned before pouring the repair mortar.

 doi:10.20944/preprints202401.2123.v1

Table 2. Mix design of geopolymer mortar.

Detail	Slag (wt.%)	Fly ash (wt.%)	Red mud (wt.%)	OPC (wt.%)	Binder/ Sand	Alkali activator		Water/ Binder
						Modulus	Content (wt.%)	
S33F33R33	33	33	33	-	2	1.2	40	0.4
S10F45R45	10	45	45	-	2	1.2	40	0.4
S15F42.5R42.5	15	42.5	42.5	-	2	1.2	40	0.4
S20F40R40	20	40	40	-	2	1.2	40	0.4
S45F10R45	45	10	45	-	2	1.2	40	0.4
S42.5F15R42.5	42.5	15	42.5	-	2	1.2	40	0.4
S40F20R40	40	20	40	-	2	1.2	40	0.4
S45F45R10	45	45	10	-	2	1.2	40	0.4
S42.5F42.5R15	42.5	42.5	15	-	2	1.2	40	0.4
S40F40R20	40	40	20	-	2	1.2	40	0.4
OPC100	-	-	-	100	2	-	-	0.4

2.4. Testing method

Splitting tensile test, two-sided shear test and three-point bending test were conducted according to GB/T 50081-2019, JGJ/T70-2009 and ASTM C293-08, respectively, to evaluate the different mechanical characteristics of the bonded interface between the repair mortar and the concrete substrate. The test procedures for the different mechanical properties are shown in **Figure 2**.

2.4.1. Splitting tensile test

As shown in **Figure 2(a)**, the dimensions of both the concrete substrate and the repair mortar used in the splitting tensile test are 150 mm×150 mm×75 mm, and the test is carried out on a 1000 kN electro-hydraulic servo machine, where the loading method is taken as displacement loading and the loading rate is controlled at 0.5 mm/min, and the test is stopped when the vertical crack runs through the entire cross-section of time. Three parallel specimens were used for each group test, and the average of the collected results was regarded as the final splitting tensile strength. The splitting tensile strength was calculated according to Eq. 1.

$$f_t = \frac{2P_u}{\pi A_t} \tag{1}$$

where f_t is the splitting tensile strength (MPa), P_u is the maximum load applied at the time of fracture damage (kN), and A_t is the bonded interface area (mm^2).

2.4.2. Two-sided shear test

As shown in **Figure 2(b)**, the implementation procedure of the double-sided shear test was referred to Momayez et al. [48], where the concentrated load was achieved by setting the mat and ensuring that the lower mat was in the same vertical plane as the top mat during loading, where the loading procedure was the same as that of the splitting tensile test. In the double-sided shear test, the dimensions of the concrete substrate were 150 mm×150 mm×100 mm, the dimensions of the repair mortar were 150 mm×150 mm×50 mm, and the dimensions of the mat were 150 mm×50 mm×20 mm. The double-sided shear strength is calculated according to Eq. 2.

 doi:10.20944/preprints202401.2123.v1

$$f_s = \frac{P_u}{2A_t} \quad (2)$$

where f_s is the double-sided shear strength (MPa), P_u is the maximum load applied at the time of fracture damage (kN), A_t is the bonded interface area (mm^2).

2.4.3. Three-point bending test

The original concrete substrate was first subjected to a three-point bending test to obtain two concrete substrates with the same dimensions to be repaired, and then the fracture surfaces were roughened and cleaned by mechanical chiseling to ensure consistent roughness. As shown in **Figure 2(c)**, two concrete substrates to be repaired were placed in a 100 mm×100 mm×400 mm steel mold, and then the repair mortar was injected into the fracture surface intersection and fully vibrated, where the width of the repaired cracks was 10 mm~15 mm. The three-point bending test is loaded in the same way as the splitting tensile test, until the specimen is loaded to complete fracture to end the test. The three-point bending strength is calculated according to Eq. 3.

$$\sigma_b = \frac{3PL}{2bd^2} \quad (3)$$

where σ_b is the three-point bending strength (MPa), P is the maximum load applied at fracture damage (N), L is the base support span (mm), b is the cross-sectional width of the specimen (mm), and d is the cross-sectional height of the specimen (mm).

2.5. Micromechanism analysis

In order to elucidate the mechanism of chemical interaction between GPM and concrete substrate, the microstructural characteristics and mineral components of the interfacial transition zone (ITZ) were determined by means of microscopic characterization (SEM and XRD tests). The core fragments of the ITZ were collected at the end of the two-sided shear test, sealed in anhydrous ethanol for 24 h to terminate the hydration behavior of the silica-aluminate material, and then dried in a desiccator at low temperature to a constant weight. The SEM test was undertaken on a ZEISS Sigma 300 field emission scanning electron microscope, and the implementation procedure was to cut the dried particles into shredded particles with a cross-sectional size of approximately 5 mm, followed by evacuation, gold spraying, and observation and analysis. The XRD test was carried out by first mechanically grinding the dried particles into a powder passing a standard sieve of 0.075 mm and then observing and analyzing them on a Rigaku Smart Lab SE fixed-target X-ray powder diffractometer, where the operating conditions were a scanning range of 5°-90° and a scanning speed of 8°/min.

3. Results and discussion

3.1. Compressive strength of geopolymer mortar

The compressive strength of the GPM under different silica-alumina raw material ratio conditions is illustrated in **Figure 3**. **Figure 3(a)** depicts the variation of compressive strength of GPM with slag content, and in general the compressive strength of GPM at different curing ages grows approximately linearly and continuously with increasing slag content. The compressive strengths of S10F45R45, S15F42.5R42.5, S20F40R40 and S33F33R33 at a curing age of 28 d were 20.3, 27.7, 35.5 and 67.9 MPa with OPC100 (32.2 MPa) as the reference control group, and the strength change rates were -36.96%, -13.98%, 10.25%, and 210.87%, respectively. It can be inferred that the increase in slag content is beneficial to the development of mechanical properties of GPM, which can be mainly attributed to the fact that slag belongs to the category of high calcium system and potentially high activity, which

 doi:10.20944/preprints202401.2123.v1

produces calcium based gel products with early-strength properties after geopolymerization reactions [49].

Figure 3(b) describes the trend of the compressive strength of GPM with the content of fly ash, which specifically demonstrates that the compressive strength of GPM gradually grows with the increase of fly ash admixture to the stage of stable and slow change with 15% of fly ash admixture as the cut-off point. The compressive strength of GPM is 63.3 MPa when the fly ash admixture is 15%, and the strength growth rate compared to cement repair mortar is 196.58%. The above results indicate that the incorporation of appropriate amount of fly ash is favourable to the improvement of mechanical properties of GPM, whereas its enhancement effect is not significant after excessive incorporation. The beneficial effects of fly ash are reflected in the enhanced geopolymerization effect and tumbling effect, which can be summarized as, on the one hand, fly ash rich in silica-alumina mineral components can provide more active silica-alumina raw materials, enhance the geopolymerization reaction process and increase the generation of hydration gel products [50], and on the other hand, fly ash with tumbling form may effectively reinforce the compatibility of GPM system, make the spatial distribution range of geopolymer gel products more fully uniform and improve the internal pore structure characteristics [51].

From **Figure 3(c)**, it can be observed that the compressive strength of GPM shows a trend of gradually increasing and then decreasing with the addition of red mud, in which the compressive strength of GPM under the condition of 20% red mud addition reaches the maximum 81.7 MPa, and the strength growth rate is 253.73% compared with that of cement repair mortar. The positive effect of red mud on the mechanical properties of GPM is reflected by the high alkalinity of red mud, which can effectively promote the precursor materials to react more fully and completely with geopolymerization, and the high specific surface area of red mud, which can be used as mineral filler to populate the residual pores in the internal structure of the specimen and enhance the structural denseness of the geopolymer [52]. It should not be overlooked that the silica-alumina component of the red mud produced by the Bayer method is less active and requires more alkali activator consumption under the same condition, resulting in a lower effective amount of precursor material subjected to activation [53], which explains why excessive incorporation of red mud leads to weakened mechanical behavior of the GPM.

In order to clarify the pattern of change of compressive strength with curing age of GPM under different silica-alumina raw material ratio conditions, the strength development coefficient (the ratio of compressive strength at curing age of 28 d to that at curing age of 7 d) was defined to quantify the variability of strength development of different types of GPM. As presented in **Figure 3(a)**, the strength development coefficient of the GPM gradually decreased with the increase of slag admixture, where the strength development coefficients of S10F45R45, S15F42.5R42.5, S20F40R40 and S33F33R33 were 0.68, 0.65, 0.62 and 0.60, respectively, which may be due to the increase of slag admixture weakening the positive effect of fly ash and red mud on the geopolymerization reaction of the precursor raw materials. As shown in **Figure 3(b)**, the strength development coefficient of GPM decreases significantly and then slowly with the increase of fly ash admixture, which can be explained mainly by the high stability of fly ash itself (particle structure denseness and surface activation energy) weakening the effective amount of alkali activator [54]. In addition, fly ash generates a chemically stable sodium-based gel product N-A-S-H under the activation of alkali activator, which plays an inhibitory role in the generation of calcium-based gel products. As indicated in **Fig 3(c)**, the trend of the strength development coefficient of the GPM with the amount of red mud admixture is similar to that of fly ash, which is mainly attributed to the inert nature of the silica-alumina mineral fraction in red mud.

 doi:10.20944/preprints202401.2123.v1

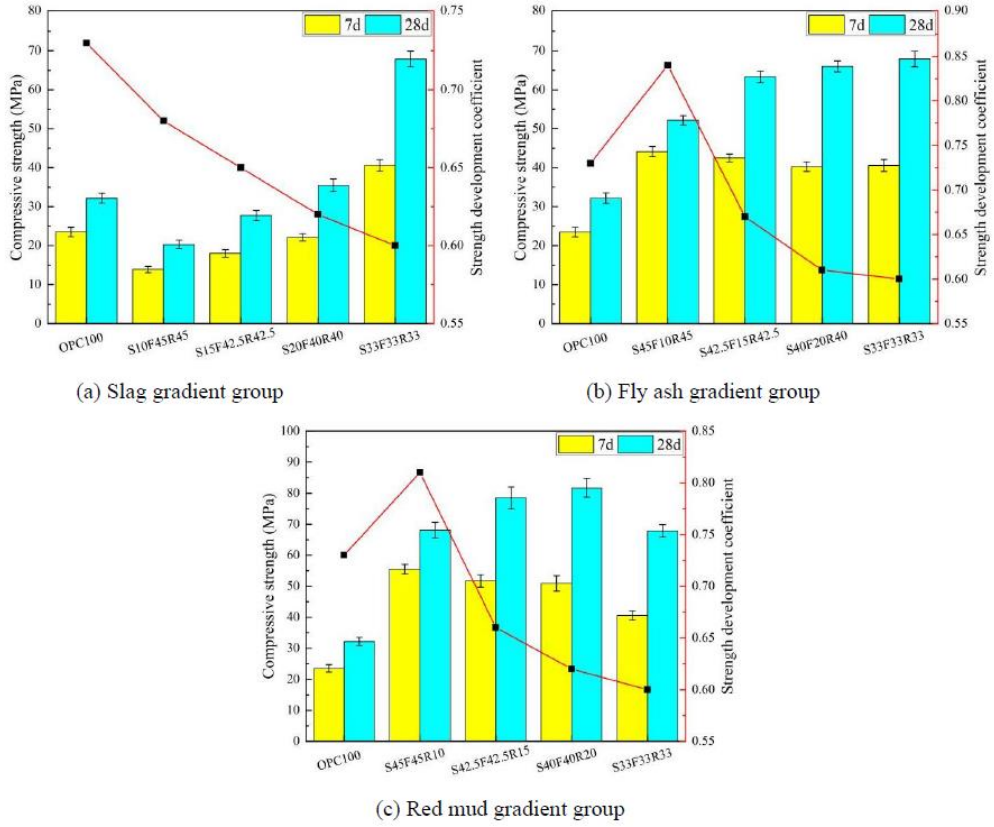

Figure 3. The compressive strength of geopolymer repair mortar.

3.2. Splitting tensile strength

The experimental results of the split tensile test are illustrated in **Figure 4**. The interfacial bond strength between the repair material and the existing concrete substrate always consists of a combination of physical, chemical or mechanical effects such as adhesive and van der Waals forces induced by the repair material, frictional resistance generated by rough interfaces, and mechanical interlocking effects between the exposed aggregates [55]. Since the surface roughness of the concrete substrate was uniform in this test, the interfacial bond strength between the GPM and the concrete substrate mainly depends on the bond mechanical properties of the GPM. As can be seen in **Figure 4(a)**, the overall split tensile strength of the GPM repaired concrete substrate continued to grow with the increase of slag content within a certain range, but a partial weakening of the split tensile strength occurred when the slag content exceeded 33%. With OPC100 as the reference group, the corresponding growth rates of splitting tensile strength for S10F45R45, S15F42.5R42.5, S20F40R40 and S33F33R33 were -5.0%, 16.3%, 35.6% and 15.0%, respectively. Unsurprisingly, the reason that the split tensile strength at 10% slag content is lower than the benchmark group is that the calcium content of the active component in the GPM system is simply too low-enough to allow for a reduction in the generation of calcium-based geopolymer gel products, resulting in a lower degree of contribution to the strength of the GPM. However, when the dosage of slag exceeds a certain threshold, the rapid hydration of the active calcium component in the slag induces the enhancement of capillary tension in the internal structure of the geopolymer gel, which enlarges the drying shrinkage of the geopolymer, thus weakening the interfacial adhesion between the GPM and the concrete substrate [56].

Figure 4(b) reveals that the splitting tensile strength of GPM and concrete substrate with different fly ash dosage is relatively higher than that of cement repair mortar under the same dosage condition, which is manifested in the fact that the splitting tensile strength rises continuously and then decreases with the addition of fly ash content. Taking OPC100 as the base group, the growth rates of split tensile strength corresponding to S45F10R45, S42.5F15R42.5, S40F20R40 and S33F33R33

 doi:10.20944/preprints202401.2123.v1

were 31.9%, 34.6%, 44.9% and 21.3%, respectively. The above results can be attributed to the favourable effects of moderate addition of fly ash in terms of geopolymerization enhancement and tumbling effect, while the unfavourable effects of excessive incorporation of fly ash are in terms of its inhibition of geopolymerisation reactions [50,51].

As shown in **Figure 4(c)**, unlike the slag and fly ash gradient groups, the increase in red mud content produces a sustained negative effect on the splitting tensile strength of the GPM repaired concrete substrate. Compared to OPC100, the growth rates of split tensile strength corresponding to S45F45R10, S42.5F42.5R15, S40F40R20 and S33F33R33 were 46.3%, 38.8%, 29.4% and 15.0%, in that order. From this, it can be judged that red mud with high alkalinity is limited to enhance the geopolymerization effect on the precursor raw materials, however, the silica-aluminium mineral components in red mud are mostly inert and difficult to participate in the geopolymerization reaction, which disturbs the pore distribution characteristics within the geopolymer restoration mortar and augments the structural porosity [53].

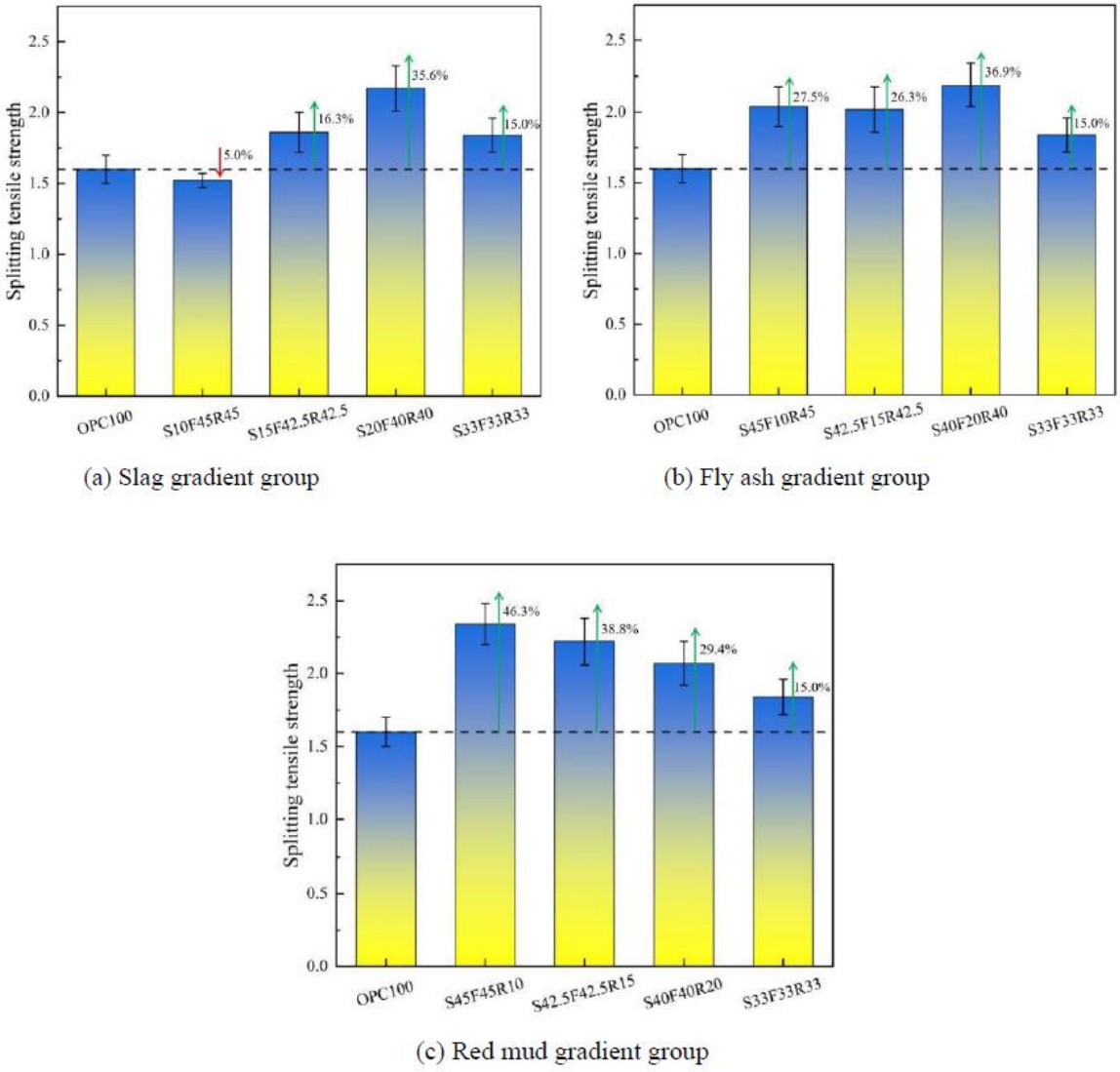

Figure 4. The splitting tensile strength of geopolymer mortar and concrete substrate.

3.3. Double-sided shear strength

Figure 5 exhibits the experimental results of GPM repaired concrete substrate after double-sided shear test. As obtained in **Figure 5(a)**, the two-sided shear strength of the bond interface between the GPM and the concrete substrate progressively enhanced with the increase of slag content. The growth

 doi:10.20944/preprints202401.2123.v1

rates of double-sided shear strength corresponding to S10F45R45, S15F42.5R42.5, S20F40R40 and S33F33R33 were -3.9%, 46.3%, 13.7% and 33.3%, respectively, with OPC 100 as the parallel control group. The above phenomenon stems from the fact that the increase in slag content promotes the production of calcium-based geopolymer gel products, which generates an "embedding effect" that effectively prevents relative shear slip damage at the interface between the GPM and concrete substrate, thus enhancing the interfacial bond between the GPM and concrete substrate [32].

As shown in **Figure 5(b)**, the pattern of change of double-sided shear strength of GPM repaired concrete substrate is negatively correlated with the growth of fly ash content, in other words, the double-sided shear strength continues to decline continuously with the growth of fly ash content. With reference to OPC100, S45F10R45, S42.5F15R42.5, S40F20R40, and S33F33R33 correspond to double-sided shear strength growth rates of 45.1%, 41.2%, 27.5%, and 33.3%, respectively. It is inferred that the available chemically stable fly ash particles exert a significant negative effect on the mechanical properties of GPM by inhibiting the geopolymerization reaction process of the precursor raw materials.

Figure 5(c) demonstrates the developmental pattern of the two-sided shear strength of the GPM repaired concrete with the growth of the red mud content in agreement with the fly ash. With respect to OPC100, the corresponding double-sided shear strength growth rates for S45F45R10, S42.5F42.5R15, S40F40R20 and S33F33R33 are 46.3%, 38.8%, 29.4% and 15.0%, respectively. The analysis shows that red mud, which is rich in a substantial amount of inactive silica-aluminium fractions, reduces the proportion of active silica-aluminium fractions in geopolymer, thereby inhibiting the development of the mechanical properties of GPM [53].

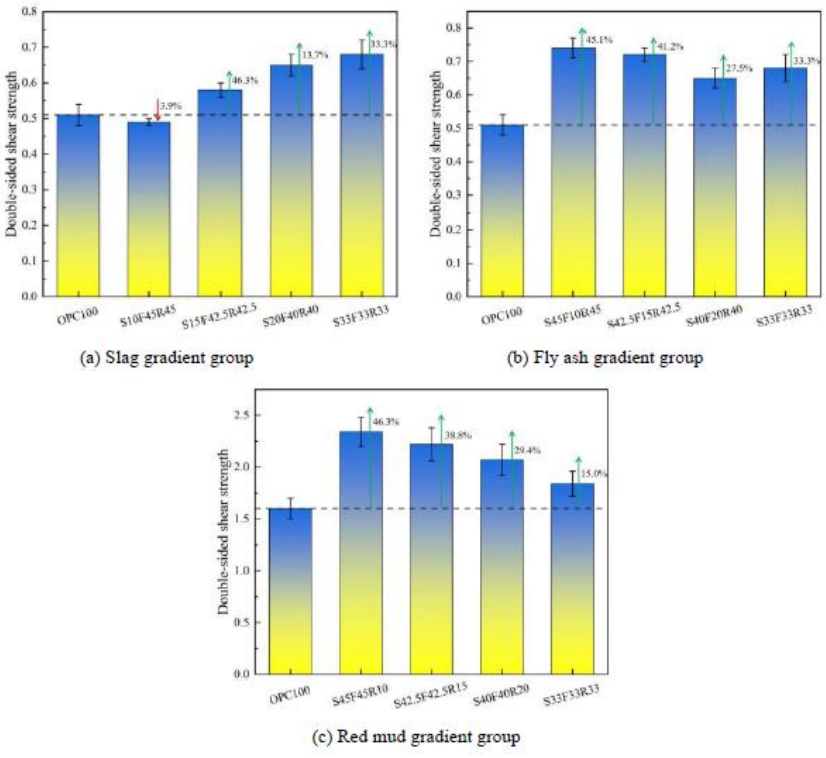

Figure 5. The double-sided shear strength of geopolymer mortar and concrete substrate.

3.4. Three-point bending strength

The experimental results of GPM repaired concrete substrate after three-point bending test are presented in **Figure 6**. As can be seen in **Figure 6(a)**, the three-point bending strength of the GPM repaired concrete substrate increases stepwise with the increase of slag content. Taking OPC100 as the reference group, the corresponding three-point bending strength growth rates for S10F45R45, S15F42.5R42.5, S20F40R40, and S33F33R33 are -18.5%, -15.0%, -21.3%, and 21.3%, respectively. The

 doi:10.20944/preprints202401.2123.v1

above results indicate that the three-point bending strength of the GPM repaired concrete substrate is lower than that of the cement repair mortar when the slag content is below a certain amount, which can be attributed to the weaker flexural than compressive properties of the calcium-based geopolymer hydration products. This is specifically manifested in the GPM repaired concrete substrate to withstand the external load once more than its interfacial cracking load, the whole will be along the destruction of the cracking surface of the continued rapid destruction, the bearing capacity is greatly reduced.

From **Figure 6(b)**, it can be obtained that the three-point bending strength of the GPM repaired concrete substrate shows a trend of sustained increase and then decrease with the addition of fly ash content. Compared to OPC100, the corresponding three-point bending strength growth rates for S10F45R45, S15F42.5R42.5, S20F40R40 and S33F33R33 are 31.9%, 34.6%, 44.9% and 21.3%, respectively. The above phenomena can be explained by the geopolymerization enhancement effect and the tumbling effect contributed by moderate amounts of fly ash leading to an increase in the generation of geopolymer gel products, especially sodium-based hydration products (N-A-S-H), and in this way facilitating the development of the flexural properties of GPM repaired concrete substrate. The inhibitory effect of geopolymerization exhibited by excessive fly ash played a major role in weakening the load bearing Behavior of the geopolymer mortar repaired concrete substrate.

Figure 6(c) depicts the three-point bending strength of GPM repaired concrete substrate with the increase of red mud content firstly decreases continuously. With OPC100 as the reference group, the corresponding three-point bending strength growth rates for S10F45R45, S15F42.5R42.5, S20F40R40 and S33F33R33 are 40.2%, 27.6%, 25.2% and 21.3%, respectively. The reason for these results is that most of the silica-aluminium mineral components in red mud are inert and not involved in the geopolymerization reaction process, thus reducing the output of geopolymer gel products and significantly weakening the load-bearing properties of the GPM repaired concrete substrate.

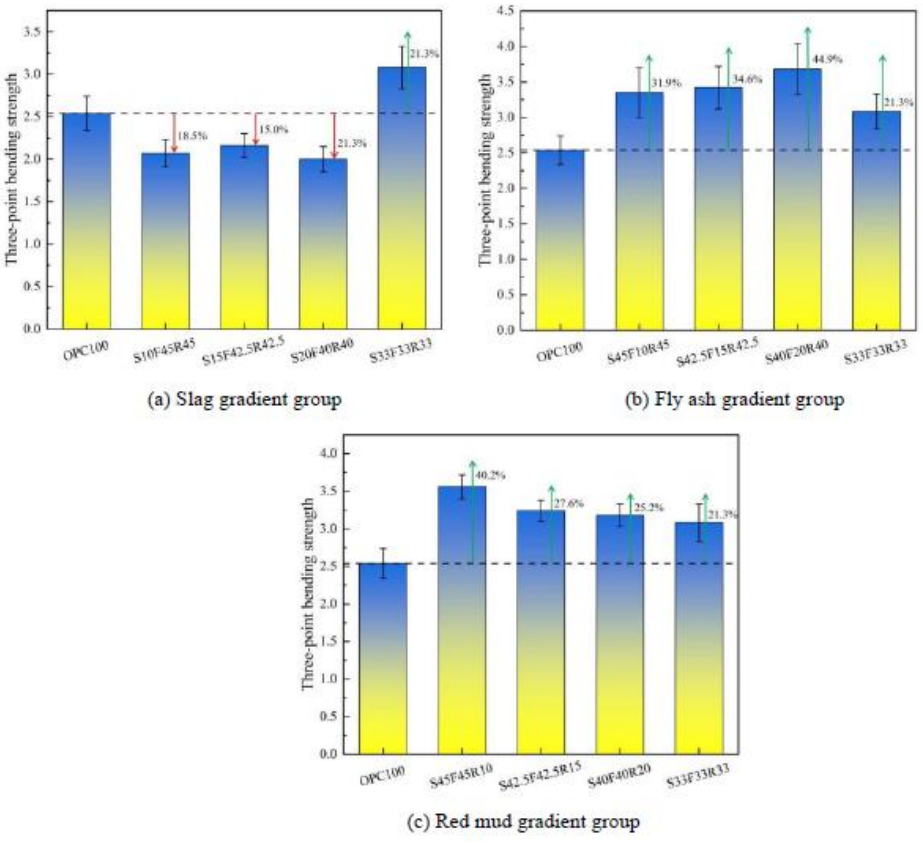

Figure 6. The three-point bending strength of geopolymer mortar and concrete substrate.

 doi:10.20944/preprints202401.2123.v1

3.5. SEM analysis

In order to further analyze the formation mechanism of interfacial bond strength of GPM repairing concrete substrate, the specimen in the ITZ after double-sided shear test was selected as the research object, and its microstructural characteristics were analyzed by SEM test. **Figure 7(a-c)** shows that the GPM with more holes of variable shapes and different distribution ranges at slag dosage not exceeding 15%, which may be attributed to the evaporation loss of water from the geopolymer gel production during the set-hardening process. In addition to this, what is noticeable is the presence of a high quantity of fly ash and red mud particles not involved in the geopolymerization reaction throughout the interior of the substrate, as well as wide cracks located close to the side of the GPM. The above findings can be interpreted as the low content of highly reactive slag could not induce enough geopolymer gel products to sufficiently bond and encapsulate the fly ash and red mud particles. As the slag content grows to 20%, the number of internal holes shrinks significantly, but traces of penetrating microcracks can still be found.

As can be seen in **Figure 7(d-f)**, the geopolymer gel products were significantly increased and the overall densification of the internal spatial structure was enhanced due to the geopolymerization enhancement effect and the ballooning effect provided by the fly ash at a dosage of less than 15%. The above results were specifically demonstrated by the fact that the ITZ between the GPM and the concrete substrate exhibited a complete continuity. However, as the fly ash content was raised to 20%, on the one hand, a limited proportion of unreacted fly ash particles gradually appeared in the internal structure, and on the other hand, there was a clear boundary between the GPM and the concrete substrate accompanied by obvious microcracks, in which the structure on the side near the concrete substrate was loose and porous. It can be concluded that excessive fly ash is detrimental to the development of the mechanical properties of GPM, resulting in a weakening of the interfacial bond to the concrete substrate.

From **Figure 7(g-i)**, it can be concluded that the red mud dosed with not more than 15% can give considerable alkalinity and physical filling effect, which makes the increasing geopolymer gel products stacked with each other, and effectively enhances the degree of structural densification. However, it is still convenient to discover some flaky adherents on the surface of the GPM substrate and microcracks in the ITZ between the geopolymer mortar and the concrete substrate. When the red mud dosage was increased to 20%, the distribution of attachments on the GPM and concrete substrate was further expanded, and the surface roughness was increased, accompanied by clearly visible pore defects. This may stem from the fact that the inert silica-aluminium mineral fraction present in the red mud does not participate in the geopolymerization reaction and only acts as a filler for the mineral particles, resulting in a significant reduction in the yield of geopolymer gels.

Figure 7(j) suggests that under the condition of slag, fly ash and red mud mixed in equal proportions, the precursor raw materials were able to generate sufficient geopolymer cementation products under the effect of excitation and activation, which possessed better mechanical bonding properties, making the ITZ between the GPM and the concrete substrate continuous and intact, but it needs to be clarified that a minority of microcracks still existed within the structure. **Figure 7(k)** reveals that compared to the GPM, the internal structure of the cement mortar is discrete and loose, with a large distribution of porous defects, which may be attributed to the random uncontrolled evaporation of water and the negative effect of self-shrinkage during the set-hardening process of the cement mortar. In addition, there are obvious cracks between the cement mortar and the concrete substrate, and the overall joint over performance is weakened, which is macroscopically manifested as a significant attenuation of the interfacial bond strength of the cement mortar repairing the concrete substrate.

 doi:10.20944/preprints202401.2123.v1

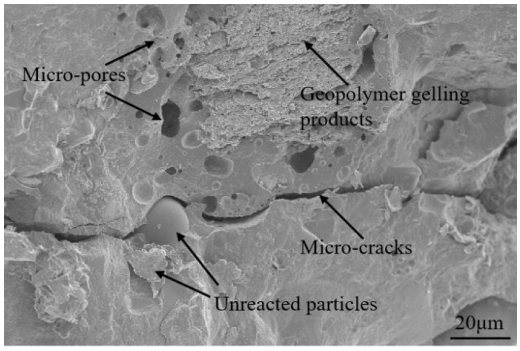

(a) S10F45R45

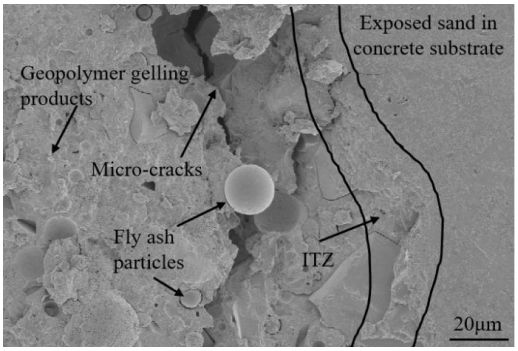

(b) S15F42.5R42.5

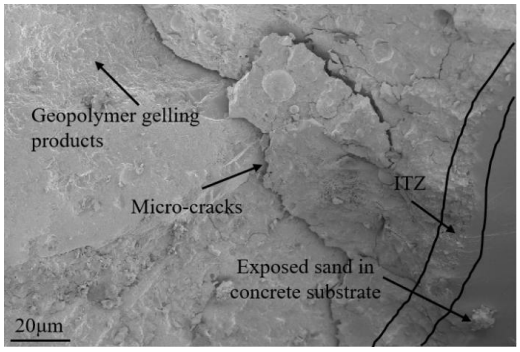

(c) S20F40R40

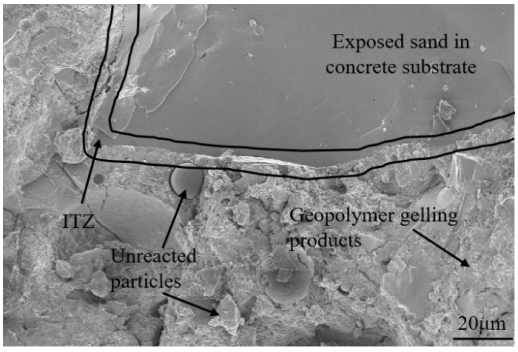

(d) S45F10R45

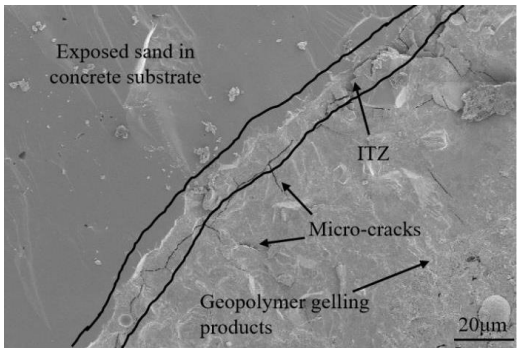

(e) S42.5F15R42.5

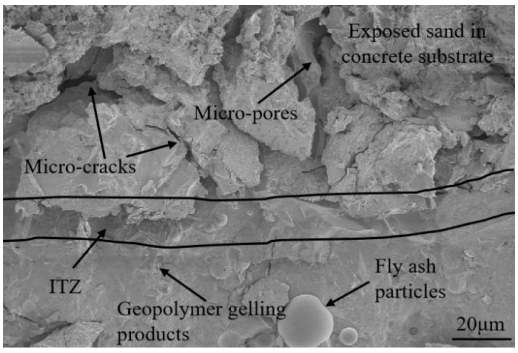

(f) S40F20R40

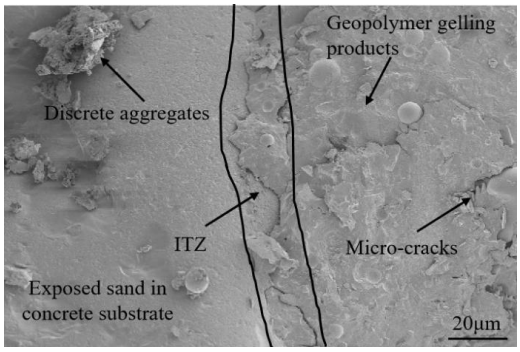

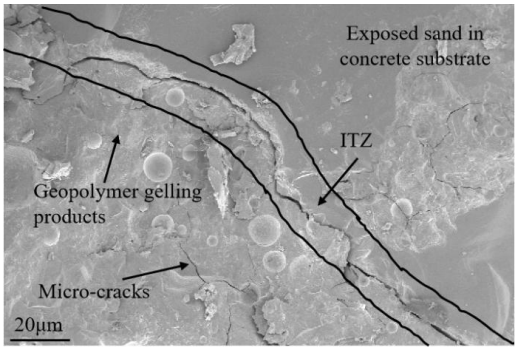

 doi:10.20944/preprints202401.2123.v1

(g) S45F45R10 (h) S42.5F42.5R15

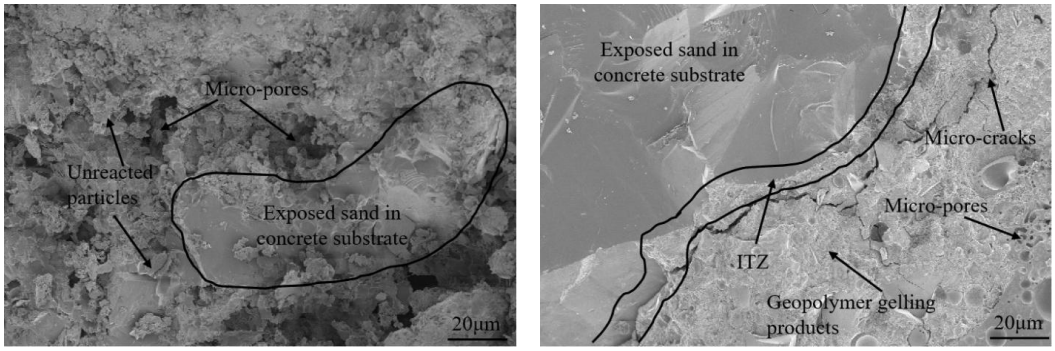

(i) S40F40R20 (j) S33F33R33

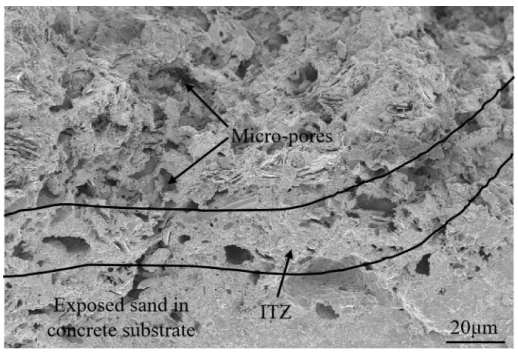

(k) OPC10

Figure 7. The SEM images of ITZ of geopolymer mortar with concrete substrate.

3.6. XRD analysis

The XRD test was carried out to investigate the physical composition of different types of GPM. The results of XRD profiles of GPM with different slag, fly ash and red mud mixing ratios are presented in **Figure 8**. **Figure 8(a-c)** exhibits that the mineral composition of each type of GPM belongs to a mixed composition of crystalline and amorphous phases. The crystalline phases of the mineral composition can be summarized as quartz, calcite and hematite, with quartz being largely derived from the fine aggregates and precursor raw materials used in the preparation of the mortar, which are classified as inert and do not take part in the geopolymerization hydration reactions. The formation of calcite may be attributed to the carbonation of calcium-based hydration products by combining free carbon dioxide and moisture in the air during standard maintenance at the end of preparation. The presence of hematite can be interpreted as the red mud prepared by the Bayer method contains a portion of Fe_2O_3 in the form of crystals, which are chemically stable and do not participate in geopolymer hydration reactions.

From **Figure 8(a)**, it can be analyzed that the intensity of the diffraction peaks of the calcium-based hydration products (C-S-H, C-A-S-H), which determine the development of the mechanical properties in GPM, is subsequently enhanced with the growth of the slag content. This also explains that the increase in slag content favours the development of bond strength at the interface between the GPM and the concrete substrate. **Figure 8(b)** demonstrates that the improvement in fly ash content heightens the production of sodium-based hydration products (N-A-S-H), but suppresses the progression of calcium-based hydration products. It can be inferred from **Figure 8(c)** that the inclusion of red mud facilitates the expansion of calcium- and sodium-based hydration products within a certain range, but once the optimal amount of inclusion is exceeded, red mud plays more of a negative role. The above mentioned results are in agreement with the outcomes of the macromechanical tests, and the addition of excessive fly ash and red mud is rather detrimental to the subsequent development of the interfacial bond strength between the GPM and the concrete

 doi:10.20944/preprints202401.2123.v1

substrate. The categories of hydration gel products in the cement mortar in **Figure 8(d)** are mainly C-S-H and C-A-H, which is in accordance with the results of previous investigations on the subject.

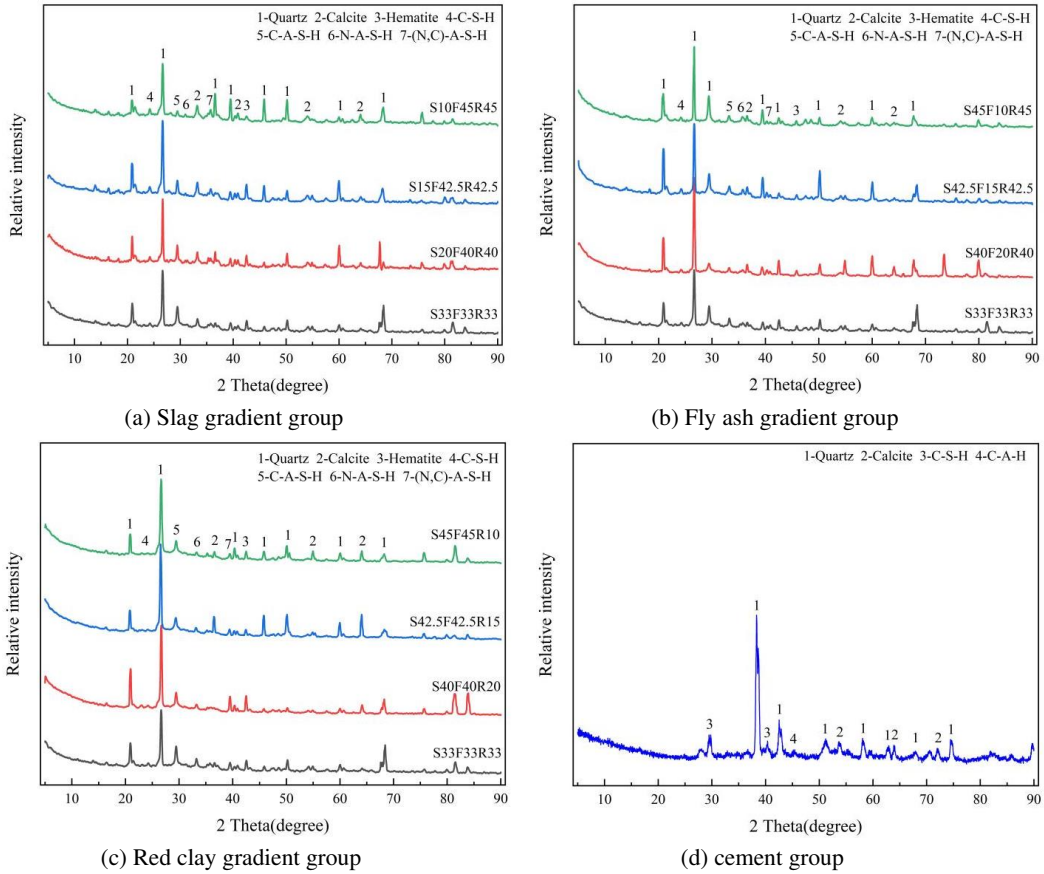

Figure 8. The XRD images of geopolymer repair mortar.

4. Conclusions

The objective of this investigation is to illustrate the influence of different slag, fly ash and red mud mixing ratio conditions on the interfacial properties of GPM and OPC concrete substrate, and to explore the interfacial bonding properties of GPM and concrete substrate by carrying out split tensile test, two-sided shear test and three-point bending test, as well as microscopic characterization means, such as SEM and XRD. Combined with the experimental results of this study, the following conclusions are drawn:

(1) The compressive strength of the GPM displays an increasing evolution with the improvement of the slag content, however, with the growth of the fly ash content it reveals a minor increase followed by a gradual levelling off. Limited amounts of red mud produce favourable effects on the compressive strength of GPM to a certain extent, whereas excessive amounts of red mud produce more of a negative effect.

(2) The splitting tensile strength of GPM and concrete substrate with the growth of slag, fly ash content all demonstrates the rule of change of the first growth and then decline, in which the fly ash presents a favourable effect is better than the slag, however, with the increase of red mud content and presents an approximate linear decline in the trend of change.

(3) The two-sided shear strength of GPM and concrete substrate exhibited a continuous improvement with the increase of slag content, however, it tended to decrease slowly with the increase of fly ash and red mud content.

(4) The three-point bending strength of GPM and concrete substrate is not as good as that of cement mortar under the condition of less slag mixing, however, with the increase of fly ash content

presents the variation tendency of increasing and then decreasing, and with the growth of red mud content exhibits a continuous decreasing trend.

Author Contributions: Conceptualization, Q.L., Y.Z. and B.Z.; Investigation, H.Y., Z.L., Z.L., G.Z. and K.L.; Writing-original draft preparation, H.Y., Z.L., Z.L., G.Z. and K.L.; Writing-review and editing, Q.L., Y.Z. and B.Z. All authors have read and agreed to the published version of the manuscript.

Funding: This research work was financially supported by the Open Research Fund of Key Laboratory of Construction and Safety of Water Engineering of the Ministry of Water Resources, China Institute of Water Resources and Hydropower Research (NO. 202109) and the Natural Science Foundation of Hunan Province (NO. 2023JJ50008).

Conflicts of Interest: The authors declare that they have no known competing financial interests or personal relationships that could have appeared to influence the work reported in this paper.

References

1. Chen, D.; Mahadevan, S. Chloride-induced reinforcement corrosion and concrete cracking simulation. *Cem. Concr. Compos.* **2008**, 30(3): 227-238.
2. Peng, L.; Zeng, W.; Zhao, Y.; Li, L.; Poon, C.; Zheng, H. Steel corrosion and corrosion-induced cracking in reinforced concrete with carbonated recycled aggregate. *Cem. Concr. Compos.* **2022**, 133: 104694.
3. Almusallam, A.A. Effect of degree of corrosion on the properties of reinforcing steel bars. *Constr. Build. Mater.* **2001**, 15(8): 361-368.
4. Gomaa, E.; Gheni, A.; ElGawady, M. A. Repair of ordinary Portland cement concrete using ambient-cured alkali-activated concrete: Interfacial behavior. *Cem. Concr. Res.* **2020**, 129: 105968.
5. Fu, C.; Ye, H.; Jin, X.; Yan, D.; Jin, N.; Peng, Z. Chloride penetration into concrete damaged by uniaxial tensile fatigue loading. *Constr. Build. Mater.* **2016**, 125: 714-723.
6. Wang, L.; Zhang, Q. Investigation on water absorption in concrete after subjected to compressive fatigue loading. *Constr. Build. Mater.* **2021**, 299: 123897.
7. Wang, P.; Mo, R.; Li, S.; Xu, J.; Jin, Z.; Zhao, T.; Wang, D. A chemo-damage-transport model for chloride ions diffusion in cement-based materials: Combined effects of sulfate attack and temperature. *Constr. Build. Mater.* **2021**, 288: 123121.
8. Ukpata, J.O.; Basheer, P.A.M.; Black, L. Slag hydration and chloride binding in slag cements exposed to a combined chloride-sulphate solution. *Constr. Build. Mater.* **2019**, 195: 238-248.
9. Shaheen, F.; Pradhan, B. Influence of sulfate ion and associated cation type on steel reinforcement corrosion in concrete powder aqueous solution in the presence of chloride ions. *Cem. Concr. Res.* **2017**, 91: 73-86.
10. Wu, L.; Farzadnia, N.; Shi, C.; Zhang, Z, Wang, H. Autogenous shrinkage of high performance concrete: A review. *Constr. Build. Mater.* **2017**, 149: 62-75.
11. Mao, Y.; Liu, J.; Shi, C. Autogenous shrinkage and drying shrinkage of recycled aggregate concrete: A review. *J. Clean. Prod.* **2021**, 295: 126435.
12. Woźniak, Z.Z.; Chajec, A.; Sadowski, Ł. Effect of the Partial Replacement of Cement with Waste Granite Powder on the Properties of Fresh and Hardened Mortars for Masonry Applications. *Materials-Basel*, **2022**, 15(24): 9066.
13. Ahmad, S.; Elahi, A.; Barbhuiya, S.A.; Farid, Y. Use of polymer modified mortar in controlling cracks in reinforced concrete beams. *Constr. Build. Mater.* **2012**, 27(1): 91-96.
14. Assaad, J.J.; Khayat, K.H. Form pressure characteristics of self-consolidating concrete used in repair. *Cem. Concr. Compos.* **2021**, 122: 104118.
15. Reggia, A.; Morbi, A.; Plizzari, G.A. Experimental study of a reinforced concrete bridge pier strengthened with HPFRC jacketing. *Eng. Struct.* **2020**, 210: 110355.
16. Valikhani, A.; Jahromi, A.J.; Mantawy, I.M.; Azizinamini, A. Experimental evaluation of concrete-to-UHPC bond strength with correlation to surface roughness for repair application. *Constr. Build. Mater.* **2020**, 238: 117753.
17. Gao, T.; Shen, L.; Shen, M.; Chen, F.; Liu, L.; Gao, L. Analysis on differences of carbon dioxide emission from cement production and their major determinants. *J. Clean. Prod.* **2015**, 103: 160-170.
18. El-Hassan, H.; Elkholy, S. Enhancing the performance of Alkali-Activated Slag-Fly ash blended concrete through hybrid steel fiber reinforcement. *Constr. Build. Mater.* **2021**, 311: 125313.

19. Duxson, P.; Fernández-Jiménez, A.; Provis, J.L.; Lukey, G.C.; Palomo, A.; Van Deventer, J.S.J. Geopolymer technology: the current state of the art. *J. mater. Sci.* **2007**, 42(9): 2917-2933.
20. Singh, B.; Ishwarya, G.; Gupta, M.; Bhattacharyya, S.K. Geopolymer concrete: A review of some recent developments. *Constr. Build. Mater.* **2015**, 85: 78-90.
21. Bakharev, T. Resistance of geopolymer materials to acid attack. *Cem. Concr. Res.* **2005**, 35(4): 658-670.
22. Davidovits, J. Geopolymers: inorganic polymeric new materials. *J. Therm. Anal. Calorim.* **1991**, 37(8): 1633-1656.
23. Huang, W.; Wang, H. Geopolymer pervious concrete modified with granulated blast furnace slag: Microscale characterization and mechanical strength. *J. Clean. Prod.* **2021**, 328: 129469.
24. Nath, P.; Sarker, P.K. Flexural strength and elastic modulus of ambient-cured blended low-calcium fly ash geopolymer concrete. *Constr. Build. Mater.* **2017**, 130: 22-31.
25. Rovnaník, P. Effect of curing temperature on the development of hard structure of metakaolin-based geopolymer. *Constr. Build. Mater.* **2010**, 24(7): 1176-1183.
26. Bature, A.S.; Khorami, M.; Ganjian, E.; Tyrer, M. Influence of alkali activator type and proportion on strength performance of calcined clay geopolymer mortar. *Constr. Build. Mater.* **2021**, 267: 120446.
27. Demir, F.; Derun, E.M. Modelling and optimization of gold mine tailings based geopolymer by using response surface method and its application in Pb^{2+} removal. *J. Clean. Prod.* **2019**, 237: 117766.
28. Ahmari, S.; Zhang, L. Production of eco-friendly bricks from copper mine tailings through geopolymerization. *Constr. Build. Mater.* **2012**, 29: 323-331.
29. Laskar, S,M.; Talukdar, S. A study on the performance of damaged RC members repaired using ultra-fine slag based geopolymer mortar. *Constr. Build. Mater.* **2019**, 217: 216-225.
30. Gomaa, E.; Gheni, A.; ElGawady, M.A. Repair of ordinary Portland cement concrete using ambient-cured alkali-activated concrete: Interfacial behavior. *Cem. Concr. Res*. **2020**, 129: 105968.
31. Zailani, W.W.A.; Abdullah, M.M.A.B, Arshad, M.F.; Razak, R.F.; Tahir, M.F.M.; Zainol, R.R.M.A.; Nabialek, M.; Sandu, A.V.; Wyslocki, J.J.; Bloch, K. Characterisation at the bonding zone between fly ash based geopolymer repair materials (GRM) and ordinary portland cement concrete (OPCC). *Materials-Basel*, **2020**, 14(1): 56.
32. Wang, Y.S.; Peng, K.D.; Alrefaei, Y.; Dai, J. The bond between geopolymer repair mortars and OPC concrete substrate: Strength and microscopic interactions. *Cem. Concr. Compos*. **2021**, 119: 103991.
33. Wang, S.; Jin, H.; Deng, Y.; Xiao, Y. Comprehensive utilization status of red mud in China: A critical review. *J. Clean. Prod.* **2021**, 289: 125136.
34. Zhao, H.; Gou, H. Unfired bricks prepared with red mud and calcium sulfoaluminate cement: Properties and environmental impact. *J. Build. Eng.* **2021**, 38: 102238.
35. Mudgal, M.; Singh, A.; Chouhan, R.K.; Acharya, A.; Srivastava, A.K. Fly ash red mud geopolymer with improved mechanical strength. *Clean. Eng. Technol.* **2021**, 4: 100215.
36. Khairul, M.A.; Zanganeh, J.; Moghtaderi, B. The composition, recycling and utilisation of Bayer red mud. *Resour. Conserv. Recy*. **2019**, 141: 483-498.
37. Atan, E.; Sutcu, M.; Cam, A.S. Combined effects of bayer process bauxite waste (red mud) and agricultural waste on technological properties of fired clay bricks. *J. Build. Eng.* **2021**, 43: 103194.
38. Kim, S.Y.; Jun, Y.; Jeon, D.; Oh, J.E.. Synthesis of structural binder for red brick production based on red mud and fly ash activated using $Ca(OH)_2$ and Na_2CO_3. *Constr. Build. Mater.* **2017**, 147: 101-116.
39. Xu, X.; Song, J.; Li, Y.; Wu, J.; Liu, X.; Zhang, C. The microstructure and properties of ceramic tiles from solid wastes of Bayer red muds. *Constr. Build. Mater.* **2019**, 212: 266-274.
40. Qaidi, S.M.A.; Tayeh, B.A.; Ahmed, H.U.; Emad, W. A review of the sustainable utilisation of red mud and fly ash for the production of geopolymer composites. *Constr. Build. Mater*. **2022**, 350: 128892.
41. Zakira, U.; Zheng, K.; Xie, N.; Birgisson, B. Development of high-strength geopolymers from red mud and blast furnace slag. *J. Clean. Prod.* **2023**, 383: 135439.
42. Liang, X.; Ji, Y. Experimental study on durability of red mud-blast furnace slag geopolymer mortar. *Constr. Build. Mater.* **2021**, 267: 120942.
43. Hertel, T.; Pontikes, Y. Geopolymers, inorganic polymers, alkali-activated materials and hybrid binders from bauxite residue (red mud)-Putting things in perspective. *J. Clean. Prod.* **2020**, 258: 120610.
44. Amran, M.; Debbarma, S.; Ozbakkaloglu, T. Fly ash-based eco-friendly geopolymer concrete: A critical review of the long-term durability properties. *Constr. Build. Mater*. **2021**, 270: 121857.

45. Guo, S.; Wu, Y.; Jia, Z.; Qi, X.; Wang, W. Sodium-based activators in alkali-activated materials: Classification and comparison. *J. Build. Eng.* **2023**: 106397.
46. Luo, Z.; Zhang, B.; Zou, J.; Luo B. Sulfate erosion resistance of slag-fly ash based geopolymer stabilized soft soil under semi-immersion condition. *Case Stud. Constr. Mat.* **2022**, 17: e01506.
47. Santos, P.M.D.; Julio, E.N.B.S. Correlation between concrete-to-concrete bond strength and the roughness of the substrate surface. *Constr. Build. Mater.* **2007**, 21(8): 1688-1695.
48. Momayez, A.; Ehsani, M.R.; Ramezanianpour, A.A.; Rajaie, H. Comparison of methods for evaluating bond strength between concrete substrate and repair materials. *Cem. Concr. Res.* **2005**, 35(4): 748-757.
49. Moudio, A.M.N.; Tchakoute, H.K.; Ngnintedem, D.L.V.; Andreola, F.; Kamseu. E.; Nanseu-Njiki, C.P.; Leonelli, C.; Rüscher, C.H. Influence of the synthetic calcium aluminate hydrate and the mixture of calcium aluminate and silicate hydrates on the compressive strengths and the microstructure of metakaolin-based geopolymer cements. *Mater. Chem. Phys.* **2021**, 264: 124459.
50. Luo, Z.; Zhang, B. Effect of humic acid and fulvic acid on mechanical and durability properties of geopolymer stabilized soft soil[J]. *Constr. Build. Mater.* **2023**, 409: 133875.
51. Nath, P.; Sarker, P.K. Effect of GGBFS on setting, workability and early strength properties of fly ash geopolymer concrete cured in ambient condition. *Constr. Build. Mater.* **2014**, 66: 163-171.
52. Khairul, M.A.; Zanganeh, J.; Moghtaderi, B. The composition, recycling and utilisation of Bayer red mud. *Resour. Conserv. Recy.* **2019**, 141: 483-498.
53. Hu, W.; Nie, Q.; Huang, B.; Shu, X.; He, Q. Mechanical and microstructural characterization of geopolymers derived from red mud and fly ashes. *J. Clean. Prod.* **2018**, 186: 799-806.
54. John, S.K.; Nadir, Y.; Girija, K. Effect of source materials, additives on the mechanical properties and durability of fly ash and fly ash-slag geopolymer mortar: A review. *Constr. Build. Mater.* **2021**, 280: 122443.
55. He, Y.; Zhang, X.; Hooton, R.D.; Zhang, X. Effects of interface roughness and interface adhesion on new-to-old concrete bonding. *Constr. Build. Mater.* **2017**, 151: 582-590.
56. Gomaa, E.; Gheni, A.; ElGawady, M.A. Repair of ordinary Portland cement concrete using ambient-cured alkali-activated concrete: Interfacial behavior. *Cem. Concr. Res.* **2020**, 129: 105968.